PCCP

Accepted Manuscript

ROYAL SOCIETY OF CHEMISTRY

rsc.li/pccp

View Article Online
DOI: 10.1039/C7CP06278H

Journal Name

ARTICLE

0.
Received 00th January 20xx,
Accepted 00th January 20xx
DOI: 10.1039/x0xx00000x

www.rsc.org/

The effect of structural modifications on the thermal stability, melting points and ion interactions for a series of tetraaryl-phosphonium-based mesothermal† ionic liquids

Cody A. Cassity,[a] Benjamin Siu,[b] Mohammad Soltani,[a] Jimmy L. McGeehee,[a] Katie J. Strickland,[a] Matt Vo,[a] E. Alan Salter,[a] Alexandra C. Stenson,[a] Andrzej Wierzbicki,[a] Kevin N. West,[b] Brooks D. Rabideau,*[b] and James H. Davis, Jr.*[a]

A family of mesothermal ionic liquids comprised of tetraarylphosphonium cations and the bis(trifluoromethanesulfonyl)amidate anion are shown to be materials of exceptional thermal stability, enduring (without decomposition) heating in air at 300°C for three months. It is further established that three specific structural elements – phenoxy, phenacyl, and phenyl sulfonyl – can be present in the cation structures without compromising their thermal stability, and that their incorporation has specific impacts on the melting points of the salts. Most importantly, it is shown that the ability of such a structural component to lower a salt melting point is tied to its ability to lower cation-cation repulsions in the material.

Introduction

During the 1960s, researchers from the United States Air Force Research Laboratory, Shell Oil Company, Monsanto, and others conducted extensive studies on the thermal stability of small organic molecules.[1-5] In broad terms, those studies established the superior thermal stability of aromatic species over those that are aliphatic in character, as well as the types of heteroatom-containing groups which tend to be thermally robust versus those which are not. Those studies were contemporaneous with successful efforts by C. S. Marvel to develop thermally robust polymers, the structural and compositional elements of which closely align with those found to be conducive to thermal stability in small molecules.[6-10] We note that several polymers invented during that period – PEEK, PES, etc. (Figure 1) – have since become commercially available, and demand for them is forecast to grow.[11]

Polymers such as those stood alone for decades as the most thermally stable organic materials known. However, in 2013 it was shown that a small number of molten salts/ionic liquids could be added to this list.[12] Specifically, ILs based upon the PPh_4^+ (tetraphenylphosphonium; TPP) cation and a handful of variants thereof were shown by us to be thermally stable organo-ion salts, amidst a growing realization in the chemical community that typical ILs are not as stable at high temperatures as is often asserted.[13] Indeed, at elevated temperatures common IL cations – including imidazoliums, quaternary ammoniums, and tetraalkylphosphoniums[14,15] – decompose by anion-involved retro-S_N2 or E2 reactions,[13] to which perarylated species would not be subject. Subsequent research further validated the high thermal stability of the parent tetraphenylphosphonium cation[16] (first investigated in an IL context by Wilkes, *et al.*),[17,18] and even more recent work has shown that triarylsulfonium salts can likewise exhibit degrees of thermal and oxidative stability superior to common ILs, as well as polymers such as PEEK and PES.[19] Finally, and most recently, we have established a hierarchy of the relative thermal stabilities of a number of anions which are or which might be used in creating thermally stable ILs.[20]

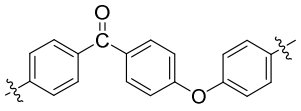

PEEK

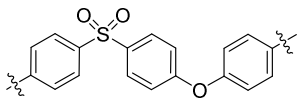

PES

Figure 1. Repeat unit structure of thermally stable polymers PEEK and PES.

Department of Chemistry, University of South Alabama, Mobile, Alabama 36688.
Department of Chemical & Biomolecular Engineering, University of South Alabama, Mobile, Alabama 36688. jdavis@southalabama.edu
Address here.

† We use the term 'mesothermal' to denote ionic liquids that do not necessarily have melting points below 100°C, but which do melt at temperatures less than those typical of purely inorganic salts, i.e., NaCl (T_m = 801°C).

Electronic Supplementary Information (ESI) available: [details of any supplementary information available should be included here]. See DOI: 10.1039/x0xx00000x

View Article Online
DOI: 10.1039/C7CP06278H

Our initial decision to explore perarylated *onium* cations as a promising basis for thermally stable ILs was prompted by the realization that these entities should be resistant to the two most common mechanistic pathways by which IL cations (heretofore regarded as the thermal weak point of ILs) are known to undergo decomposition: de-quaternization by the S_N2 or E2 cleavage of an organic appendage from the heteroatom centre of positive charge of the onium ion in question.[13] But, frustratingly, these ions are also large and rigid, factors that doubtlessly contribute to the relatively high melting points (usually > 100 °C) their salts typically exhibit. Consequently, we made early efforts to depress T_m by grafting alkyl substituents (in particular) onto one or more of the arene rings of the parent peraryl *onium* cation frameworks. It was our hope that doing so would induce T_m depression by decreasing the cation symmetry and perhaps by increasing their number of energetically accessible rotational/vibrational modes. However, it quickly (and, in retrospect, unsurprisingly) became apparent that the thermal stability of these salts was subject to the same 'rules' found by Marvel and others to govern the thermal stability of polymers and organic small molecules; in short, aliphatic substituents were thermally unstable at the high temperatures of particular interest to us (>200°C). This was also true for a large number of other possible organic functional group types.[6-10, 12]

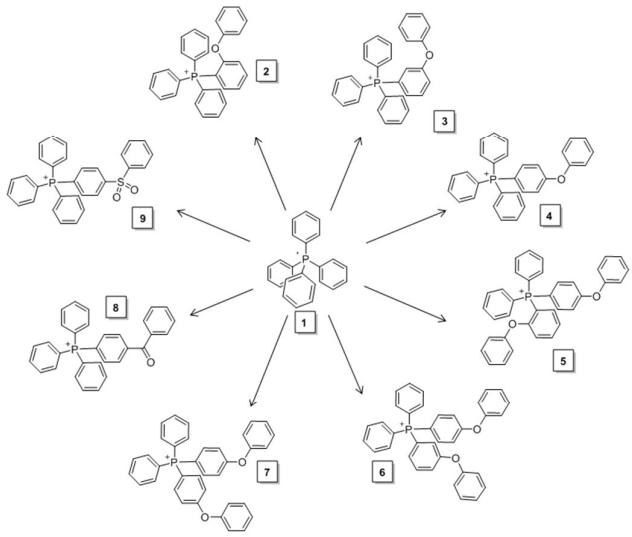

Figure 2. Structures of cations in mesothermal ionic liquids **1**-**9**. The counter-ion of each of these species was Tf_2N^- [bis(trifluoromethanesulfonyl)amidate].

Nevertheless, by happenstance we had also prepared IL **4** (Figure 2) in our initial structure-property screening activities.[12] Despite bearing an appended phenoxyether group, it, like the parent PPh_4Tf_2N salt (**1**), proved to be quite thermally stable. Better still, inclusion of the phenoxyether substituent imbued **4** with a lower T_m. Bearing in mind Marvel's work, we note that the phenoxyether functional group in **4** was one observed by him to be thermally robust when used in polymers.[6-10] Considering the foregoing, it seemed useful to undertake the synthesis of additional PPh_4^+ derivatives to further explore the connection between cation core-structure functionalization, thermal stability, and salt T_m. Our efforts have focussed on further elaboration of cation structures using phenoxy appendages, but also on diarylketone and sulfone groups (as access to requisite starting materials permit). The latter two appendage types are likewise known through high-temperature polymer research to be thermally robust. Once prepared, each new salt was to be subjected to thermal stressing for a 90-day period, in air, at 300°C, and assessed for mass loss and changes in chemical composition or structure (our now-standard methodology for assessing thermal stability).[12,19,20] Here we report the results of this study.

Experimental

Materials and representative synthesis

Commercial reagents were obtained from Aldrich Chemical, Frontier Scientific, and TCI and used without further purification. ^1H, ^{19}F, ^{31}P, and ^{13}C NMR were recorded on a 500 MHz JEOL spectrometer using $CDCl_3$ as a solvent at room temperature. All chemical shifts for ^1H and ^{13}C NMR were reported downfield using tetramethylsilane (TMS, at δ = 0.00 ppm). Mass spectra were obtained using a Thermo Scientific ion trap mass spectrometer set to positive mode ESI-MS with a mobile phase of 100% LC-MS grade methanol. Elemental analyses were obtained as a commercial technical service from Atlantic Microlabs, Inc., Norcross, Georgia, USA.

Representative synthesis: TPP-*p*-POP·Tf_2N, IL 4

A large, thick-walled, high-pressure glass tube with a PTFE screw-cap was charged with a magnetic stir bar and 5.00g (0.0191 mol) triphenylphosphine, 5.00g (0.0200 mol) 4-bromodiphenyl ether, 0.13g (0.0006 mol) anhydrous $NiBr_2$, and 6.5 mL of ethylene glycol. The combination was agitated for approximately 5 min using a mechanical vortex mixer to improve the homogeneity of the reactant mixture. The tube was then immersed in a thermostatically controlled oil bath heated to 180°C. The degree of immersion was such that all of the tube contents were below the level of the heated oil in the bath. Note that per Marcoux and Charette, careful temperature control is important for an optimal outcome.[21]

The tube and its contents were heated at 180°C for 4 h after which time the tube was carefully removed (***Caution: dangerously hot!***) from the oil bath and allowed to cool to ambient temperature. After cooling, the tube was charged with ca. 10 mL of saturated aqueous NaBr and ca. 15 mL of CH_2Cl_2 and thoroughly agitated. After allowing the aqueous and organic phases to separate, the aqueous phase was removed using a separatory funnel and the organic phase recovered and washed twice more with aqueous NaBr. After the final separation, the organic phase was dried over anhydrous Na_2SO_4, the latter removed by filtration, and the organic phase evaporated to dryness, leaving a white solid presumed to be the bromide salt of the desired cation (8.28g, 0.0162 mol, 84.8% yield (unoptimized).

Without further purification, the white solid from the previous step was suspended in 50 mL of near-boiling water. While

View Article Online
DOI: 10.1039/C7CP06278H

stirring the suspension, small portions of methanol were added until the solid was completely dissolved. Then, to the stirred, hot solution was added, in one portion, 50 mL of an aqueous solution of KTf_2N (5.80g, 0.0182 mol, 20% molar excess). A white suspension formed instantly. Upon cooling (but with continued stirring) the suspension coalesced into a dense, viscous ivory oil. The aqueous supernatant was decanted, the oil taken up in CH_2Cl_2 and dried over Na_2SO_4. After removal of the latter by filtration, the CH_2Cl_2 was removed using a rotary evaporator to produce a clear, viscous ivory oil. Over the course of about a week at ambient temperature, the oil solidified into a polycrystalline white mass (10.84g, 0.0152 mol, 94.0%). T_m (DSC): 102.1°C. Anal. calcd. for $C_{32}H_{24}F_6NO_5PS_2$: C, 54.01; H, 3.40; N, 1.97. Found: C, 54.27; H, 3.42; N, 1.96. NMR: ^{1}H ($CDCl_3$, 500 MHz): δ 7.82-7.88 (m, 3H), (m, 2H), 7.69-7.77 (m, 6H), 7.55-7.63 (m, 6H), 7.45-7.53 (m, 2H), 7.38-7.44 (m, 2H), 7.16-7.26 (m, 3H), and 7.10-7.14 (m, 2H) ppm; ^{13}C ($CDCl_3$, 125 MHz): δ 164.14, 153.60, 136.45(d), 135.40(d), 133.99(d), 130.45(d), 130.24, 125.66, 120.70, 119.33(q; C-F), 118.49, 117.69(d), 108.72(d) ppm; ^{31}P ($CDCl_3$, 202 MHz): δ 23.22 ppm. ^{19}F ($CDCl_3$, 470 MHz): δ -78.61 ppm. All other new salts were prepared in an analogous manner. Complete characterization data for them is provided as Supporting Information.

Mass spectroscopy

Approximately 2 mg samples of each salt collected before and after heating were added to 1 ml of LC-MS grade methanol in microcentrifuge tubes. The samples were then agitated in an ultrasonic bath for 15 minutes before being centrifuged for 2 minutes. Any sample that did not fully dissolve was set aside to reach saturated concentration. All samples were diluted by a factor of 10^4 by serially diluting 10 μL of solution to 1 ml using LC-MS grade methanol. After each dilution the ultrasonic agitation and centrifugation steps were repeated.

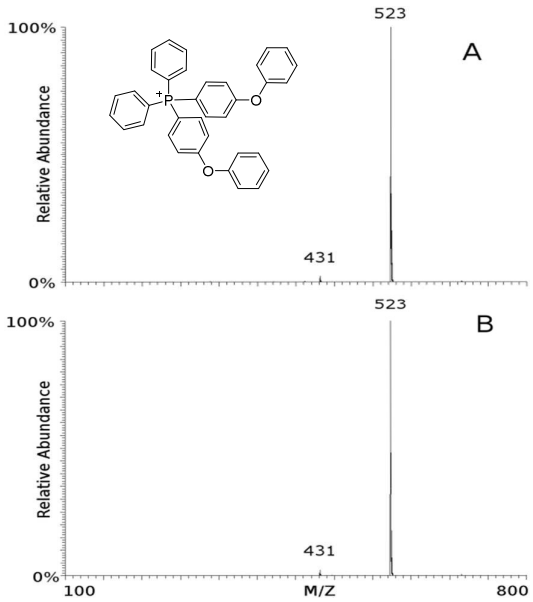

Figure 3. Positive mass spectra of IL **7** before (A) and after (B) heating in air at 300°C for 90 days.

The samples were analyzed using a Thermo Scientific ion trap mass spectrometer set to positive mode ESI-MS with a mobile phase of 100% LC-MS grade methanol. Mass spectra of samples before and after long term heat exposure were compared to confirm the presence of the parent cation and detect any compositional changes possibly caused by thermal degradation. An example spectrum is shown in Figure 3. Any peaks that could be degradation products were compared to a list of precursor materials and potential molecular fragments that could have been produced during ionization.

Differential scanning calorimetry

Melting points, glass transitions and enthalpies of fusion were measured using Differential Scanning Calorimetry (DSC) on a TA Instruments Q2000. Entropies of fusion were calculated as the enthalpy of fusion divided by the absolute temperature. In this work, the melting points are reported as the transition from a solid state (crystalline or amorphous) to the isotropic liquid state. 1-20 mg samples were loaded into open DSC pans and heated to 110°C for 10 minutes to remove any water absorbed from the environment or volatile contaminants. The samples were then cooled to -80°C and heated at a ramp rate of 10°C/minute to 300°C. Their melting points are reported as the melting onset temperature as calculated by the analysis software. All measurements were carried out under a nitrogen atmosphere. The reported values are the average of at least 3 measurements and the standard uncertainty is calculated as the standard deviation of the mean.

Thermogravimetric analysis

TGA curves were measured on a Netzsch TG 209 F1 thermal gravitational analyzer. Samples of 1-20 mg were loaded into open ceramic TGA pans and heated at 10°C per minute from ambient to 500°C under air. The reported decomposition temperatures are calculated as the onset temperature (T_{onset}) after any solvent losses.

Evaluation of long-term thermal stability

Per the procedure utilized in our prior studies – one modelled on that of Fox and co-workers[22] – on longer-term IL thermal stability, samples (0.20g – 0.50g) of each salt were charged into new 15 mL porcelain crucibles (which were left uncovered), then heated in a muffle furnace at 300°C in air for 90 days. At the end of the thermal stressing regimen the samples were removed from the oven, cooled to ambient temperature, and weighed to determine what mass loss, if any, had occurred. Further, the appearance of each sample was noted, and a complete new panel of NMR spectra (^{1}H-, ^{13}C-, ^{31}P-, and ^{19}F-NMR) and ESI-MS was obtained on each. The mass loss data for the compounds is given in Table 1.

Quantum-based calculations

View Article Online
DOI: 10.1039/C7CP06278H

The isolated cations were optimized in the gas phase using the B3LYP density functional method[23-26] and the 6-31G* basis set as implemented in Spartan '08 (Wavefunction, Inc., Irvine, CA); isodensity electrostatic potential energy maps (elstats) were then generated. All structures except **5**-**7** were confirmed as stable by computing analytic vibrational frequencies. Dipole moments were computed using Gaussian16 (Gaussian, Inc., Wallingford, USA), with the origin placed at the center of nuclear charge (as is default).

Molecular Dynamics (MD) Methodology

Liquid-phase MD simulations of IL systems were carried out under the general AMBER force field (GAFF)[27] applied to both anions and cations. Charges were derived using the Restrained Electrostatic Potential (RESP)[27] procedure, utilizing the Hartree-Fock model and 6-31G* basis set in Gaussian09 (v.09, revision E.01, Gaussian, Inc., Wallingford, USA).[28] Additionally, all charges were scaled by 80%, since it was recently shown that GAFF can accurately determine thermodynamic and transport properties of many ILs when this is done.[29] For each system, 105 IL pairs were placed inside a cubic simulation box with a side length of 55 Å using PACKMOL.[30] Simulations were performed in LAMMPS[31] using periodic boundary conditions and a 12 Å cut-off. Long-ranged electrostatic interactions were calculated using the particle-particle particle-mesh (PPPM)[32] technique with an accuracy of 10^{-4}. The system was first minimized using a conjugate gradient method until the relative changes in the energy were less that 10^{-4}. This was followed by an equilibration run in the *NPT* ensemble at 500 K and 1 atm for 1 ns using a time step of 1 fs. Corresponding damping parameters of 100 fs and 1000 fs were used to maintain the temperature and pressure, respectively. The production run consisted of a slow cooling of the system from 500 K to 400 K over the course of 20 ns. Thermodynamic data were collected every 100 fs and structural data every 20 ps for later analysis.

Results and discussion

The structure of each IL cation is shown in Figure 2. All were isolated and studied as Tf_2N^- salts, that anion having recently been established in separate work to be stable at high temperatures for long periods of time.[14] Save for the parent salt **1**, one of three functional group types was tethered to the various salt PPh_4^+ cation cores: phenoxy, phenyl ketone, or phenyl sulfone. Aided by the commercial availability of the requisite building blocks, we were able to prepare a wider assortment of phenoxy ether variants (**2**-**7**) than those with phenyl ketone (**8**) or phenyl sulfone (**9**) substituents.

The various phenoxy-appended cations, in turn, may be placed into one of two subcategories. In the first, a single phenoxy ether appendage was attached (respectively) in positions *ortho*, *meta*, and *para* to the tetraphenylphosphonium core, allowing us to determine what effects (if any) this type of positional variation alone might have on the characteristics of the resulting salts (**2**, **3**, and **4**). The second subcategory of phenoxy-modified materials were ones in which two phenoxy substituents were appended to each cation core, one of which was *p*-phenoxy in all cases (using commercially sourced by specially-made diphenyl(*p*-phenoxyphenylphosphine),[§] while the position of the second phenoxy group was varied from *ortho* to *meta* to *para* (**5**, **6**, and **7**, respectively). It was our expectation that the incorporation of two potentially 'floppy' appendages might lead to still lower values of T_m than the inclusion of just one. Characterization data for all final products (^{1}H-, ^{13}C-, ^{31}P-, and ^{19}F-NMR, ESI-MS, DSC, TGA, and CHN analysis) are provided as Supporting Information.

Table 1. Mass loss from open containers over 90 days at 300°C versus T_{onset}

Compound	Mass loss (%)	T_{onset} (°C)
1	11.2	416
2	25.0	434
3	47.6	440
4	9.5	443
5	22.0	*a*
6	21.6	*a*
7	22.2	*a*
8	10.3	447
9	0.0	436

a TGA data were acquired at the request of a reviewer after our initial experiments were concluded. By that time, no sample of compound **5**, **6**, or **7** remained. In addition, their synthesis requires a specialty starting material, all of which was likewise exhausted by that point.

Thermogravimetric Analysis and Long-term Thermal Stressing

A recent study[16] carried out by collaborators of ours in Germany clearly established two key points pertinent to the present class of ILs. First, the primary mode of thermal mass loss for the parent salt PPh_4^+ Tf_2N^- (**1**) is demonstrably evaporation *without* decomposition. Second, when IL **1** *is* thermally pushed to the point of decomposition (which occurs at temperatures >400°C), the Tf_2N^- anion decomposes while the cation remains intact. This conclusion is manifestly apparent on the basis of the comparative decomposition temperature of **1** versus $CsTf_2N$, the cation of which clearly cannot decompose. With both of these materials, a strong mass loss onset is seen around 420°C, only ascribable under the circumstances to the decomposition of Tf_2N^-. Quite significantly, as shown in Table 1, the T_{onset} of the present new ILs is in the same thermal regime. Accordingly, it seems apparent that with them as well, anion decomposition is responsible for mass losses occurring above ca. 400 °C.

Insofar as the 300°C thermal behaviour of bulk samples of the materials is concerned, Table 1 indicates that the relative thermal stabilities of the compounds varied widely, at least as measured from the standpoint of mass loss. Out of ten total materials, four had mass losses of ca. 10% or less (**1**, **4**, **8**, **9**), while others reached as high as 50% (**3**). However, in light of the paper by Wasserscheid *et al.*[16] and the TGA data for the new ILs, it seems apparent that the open-container, bulk-material mass losses experienced by ILs **2**-**9** are evaporative in character, as opposed to being by thermal decomposition followed by the volatilization of the ensuing decomposition products. To further validate this possibility, samples of the ILs

View Article Online
DOI: 10.1039/C7CP06278H

were heated to 300°C for 90 days, still under air, but in loosely capped weighing bottles. The outcome was revealing. When cooled and opened, there was essentially no mass loss (<2% with any compound), as would be expected had gaseous by-products of thermal decomposition formed and accumulated in the container. Furthermore, NMR analysis of the materials indicated that no changes in them occurred during the course of the thermal stressing. We thus conclude that the mass loss associated with these salts during the open-vessel heating was from evaporation of 'intact' ions, and not by-products of their thermal decomposition. The distinction is not trivial; such a result would suggest that the long-term thermal stability of these ILs in practical closed-system applications (cooling systems, hydraulics, etc.) could be very high indeed.

As might be the case with any IL, a larger liquidus range is likely to make for a more versatile material. Consequently, we are eager to ascertain if we can identify structure-property relationships that will allow us to reach lower pour point values with future IL designs without compromising high thermal stability. Accordingly, as was the case in a recent study focussed on high-T-stable triarylsulfonium ILs, the present compounds provided us another opportunity to conduct an exhaustive thermodynamic analysis of their the entropic and enthalpic contributions to these compounds' melting points and to couple this analysis with insight from quantum and molecular dynamics calculations.

Thermodynamics of Melting

Figure 3 shows the DSC curve for **1**, **2** and **4**, compounds which contain the parent ion and the *o*-POP and *p*-POP substitutes cations, respectively. In Figure 4, the DSC curves demonstrating weak glass transitions for compounds comprised of the *m*-POP (**3**), *o*,*p*-di-POP (**5**) and *m*,*p*-di-POP (**6**) substituted cation are shown. Lastly, the melting phenomena observed on the DSC curves for bistriflimide salts of the *p*,*p*-di-POP (**7**), the benzoyl (**8**) and the *p*-phenylsulfonyl (**9**) substituted cation are shown in Figure 5.

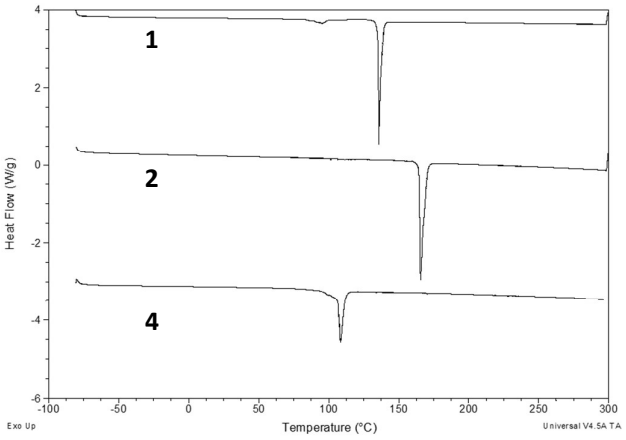

Figure 3. DSC curves for compounds **1**, **2** and **4**. The lines have been offset but not rescaled.

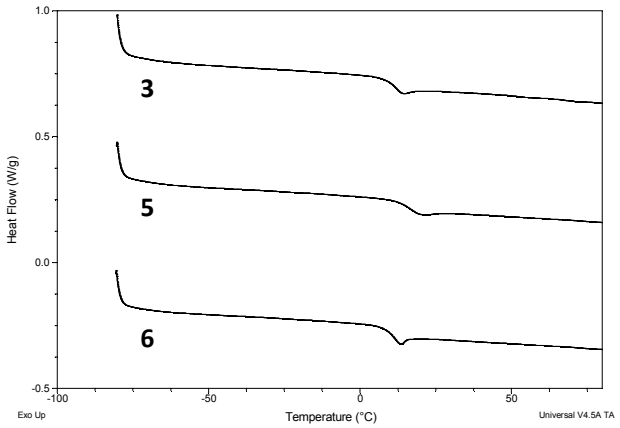

Figure 4. DSC curves for compounds **3**, **5** and **6**. The lines have been offset but not rescaled. Note that the y-axis scale is significantly smaller than for Figures 5 and 7, due to the weak nature of the thermal events.

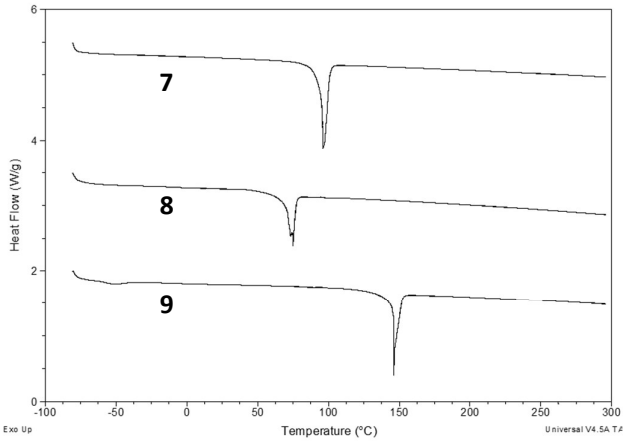

Figure 5. DSC curves for compounds **7**, **8** and **9**. The lines have been offset but not rescaled.

Table 2 shows the melting points and enthalpies and entropies of fusion for compounds **1**, **2**, **4**, **7**, **8** and **9**; the properties of compound **1**, $(Ph)_4P^+Tf_2N^-$, are included as reference so that the impact of the replacement of one of the phenyl groups with a phenoxyphenyl [POP] moiety in the parent cation can be assessed. With replacement of one phenyl group by *o*-phenoxyoenyl [*o*-POP], the new salt (**2**) has a melting point ~30°C higher than that of **1**. However, replacing one phenyl group by *p*-POP (**4**), the melting point decreases by ~33°C. We note that compounds **3** (phenyl replaced by *m*-POP), **5** (dual replacement of phenyls by *p*-POP and *o*-POP) and **6** (dual replacement of phenyls by *p*-POP and *m*-POP) were not observed to exhibit a strong transition from an ordered solid to an isotropic liquid, although weak, low-temperature glass transitions were observed for them at 10.1°C, 20.4°C, and 7.9°C, respectively, and these varied as much as 10°C depending on the thermal history of the sample. This behaviour is likely due, in part, to the asymmetry of the cation

View Article Online
DOI: 10.1039/C7CP06278H

frustrating solid-phase packing, resulting in the formation of a matrix that ossifies into an amorphous solid at low temperatures. Interestingly, and a bit surprisingly, **7**, with two *p*-POP groups on the central phosphorous, has a melting point very close to that of the **4**, which has only one *p*-POP group. Finally, for the salt containing the *p*-benzoyl group (**8**) the melting point decreases by ~61°C relative to **1**, while for the salt with the *p*-phenylsulfonyl unit (**9**), the melting point increases by 8°C.

Table 2. Melting points, enthalpies and entropies of fusion for salts **1**, **2, 4**, **7**, **8** and **9**, along with standard uncertainties as calculated by the standard deviation of the mean.

Compound	Cation	T_m (°C)	T_m (K)	± u_c (K)	ΔH^{fus} (kJ/mol)	± u_c (kJ/mol)	ΔS^{fus} (J/mol K)	± u_c (J/mol K)
1	PPh_4^+	135.0	408.2	±0.1	32.3	±0.1	79.2	±0.3
2	PPh_3-*o*-POP^+	164.7	437.9	±0.1	50.5	±0.4	115.4	±0.9
4	PPh_3-*p*-POP^+	102.1	375.3	±0.2	33.8	±0.3	90.1	±0.8
7	PPh_2-(*p*-$POP)_2^+$	94.8	368.0	±0.8	34.9	±0.5	94.9	±1.5
8	PPh_3-Ph-*p*-CO-Ph^+	73.6	346.8	±0.4	19.6	±0.4	56.5	±1.1
9	PPh_3-Ph-*p*-SO_2-Ph^+	143.0	416.2	±1.2	22.1	±0.7	53.1	±1.7

As the foregoing behaviours are more complex than as to be explained by manifestly obvious structure/property relationships, we decided to employ a combination of thermodynamic analysis, quantum calculations and molecular dynamics simulations to help clarify how the structural variations between these cations result in the observed outcomes.

For solid/liquid equilibrium at the melting point, the Gibbs free energy of fusion is 0, and the relationship between the melting point and enthalpy and entropy of fusion is given by:

$$T_m = \frac{\Delta H^{fus}}{\Delta S^{fus}}$$

Thus, relative difference in ΔH^{fus} and ΔS^{fus} for a series of similar compounds can help to reveal the influences of structural changes on T_m. To facilitate comparisons, relative changes in melting points are shown in Table 3 along with the ratios of the ΔH^{fus} and ΔS^{fus} where in salts **2**, **4** and **7** are compared to salt **1**, and **8** and **9** are compared to **4**. The latter are all *para* substituted, and only the link between the phenyl rings varies: **4**, an oxygen atom; **8**, a carbonyl group; **9**, a sulfonyl group.

Although most of the comparisons show significant changes in both ΔH^{fus} and ΔS^{fus}, the changes are (paradoxically) in the same direction and nearly offset one another in driving change in T_m.

The first entry in Table 3 shows the relative change in ΔH^{fus} and ΔS^{fus} when one of the four phenyl groups in the cation of **1** is replaced by an *o*-POP group (**1**→**2**). Both increase significantly (56% and 46%, respectively). The increase in ΔS^{fus} for the *o*-phenoxy substituted cation, even relative to the *p*-phenoxy substituted cation (discussed below) may be attributed to additional asymmetry introduced because the *ortho* position imposes a "kink" in the cation structure, similar to the way in which *cis*-double bonds or thioether moieties impose a kink in long chain alkanes, phenomena that our group has used in the past to lower the melting points of lipidic ionic liquids.[32,33] However, in the present materials this increase in ΔS^{fus} is overwhelmed by an increase in enthalpy, resulting in a melting point increase that is, in the final analysis, enthalpically driven.

Table 3. Comparison of the effects of structural variations on the thermal and thermodynamic properties of fusion for salts **2, 4,** and **7** relative to **1,** and **8** and **9** relative to **4**, and analysis of the dominant driving force for the effects. Although a driving force can be ascertained, each of the comparisons has enthalpy and entropy changes of the same magnitude which are nearly offsetting.

Comparison i vs. ref	$\Delta T_{ref \rightarrow i}$ (K)	$T_{m,i}/T_{m,ref}$ x 100%	$\Delta H^{fus,i}/\Delta H^{fus,ref}$ x 100%	$\Delta S^{fus,i}/\Delta S^{fus,ref}$ x 100%	Driving Force
2 vs. **1**	+29.7	107%	156%	146%	Enthalpically driven T_m increase
4 vs. **1**	-32.9	92%	105%	114%	Entropically driven T_m decrease
7 vs. **1**	-40.2	90%	108%	120%	Entropically driven T_m decrease
8 vs. **4**	-28.5	92%	58%	63%	Enthalpically driven T_m decrease
9 vs. **4**	+40.9	111%	65%	59%	Entropically driven T_m increase

View Article Online
DOI: 10.1039/C7CP06278H

Journal Name

ARTICLE

Additional insights into the origin of the increases in ΔS^{fus} and ΔH^{fus} are provided by quantum calculations and molecular dynamics simulations (*vide supra*).

Conversely, when the phenoxy group is introduced *para* (1→4), there is only a modest 5% increase in the ΔH^{fus}, likely due to weaker cation-anion interactions interactions arising from the presence of the *p*-phenoxy group. Likewise, the ΔS^{fus} increases by a modest 14%, thus driving the melting point decrease (entropically). Our interpretation is that asymmetry introduced by the addition of the *p*-phenoxy group likely frustrates packing in the solid phase, a phenomenon often associated with melting point decreases.

Notably, addition of the phenoxy group in the *para* position leads to an enthalpy increase that is 10 times smaller than substitution in the *ortho* position. Thus, it seems apparent that the increase in ΔH^{fus} for **2** relative to **1** cannot simply be due to increased intermolecular forces brought about by additional van der Waals interactions involving the structurally and compositionally identical added groups. In fact, computational results (below) indicate that the dominant interaction driving this change concerns cation-cation interactions, which are significantly more repulsive in **2** than they are amongst the other cations. Interestingly, compound **7**, which is structurally similar to **4**, save that it has two *p*-POP groups, has nearly identical T_m, ΔH^{fus} and ΔS^{fus} values compared to those of **4**, indicating that the introduction of an additional *p*-POP group has little thermodynamic effect.

The second set of comparisons provided in Table 3 relate **8** and **9** to **4**, and serve to elucidate the effect of the linking group type on the properties, rather than the ring position of the linking group. Both **8** and **9** have a more polar linking group than **4**; however, the effects of the structural alteration are quite different and illustrate the complexity of analysing even subtle structural changes for these species. For the **4→8** comparison, the replacement of the oxygen linkage with a carbonyl group results in a significant melting point decrease of ~29°C, with decreases in both ΔH^{fus} and ΔS^{fus}. The ΔH^{fus} of **8** is 58% of that of **4** while the ΔS^{fus} is 63% that of **4**, indicating that both were significantly altered. However, the enthalpy was decreased more, resulting in a melting point decrease that is enthalpically driven. Similarly, both the ΔH^{fus} and ΔS^{fus} of **9** decreased relative to **4**, with values that are 65% and 59%, respectively, of those of **4**. Conversely, since the entropy decrease was larger (entropically driven), the melting point increased (ΔT ~41°C).

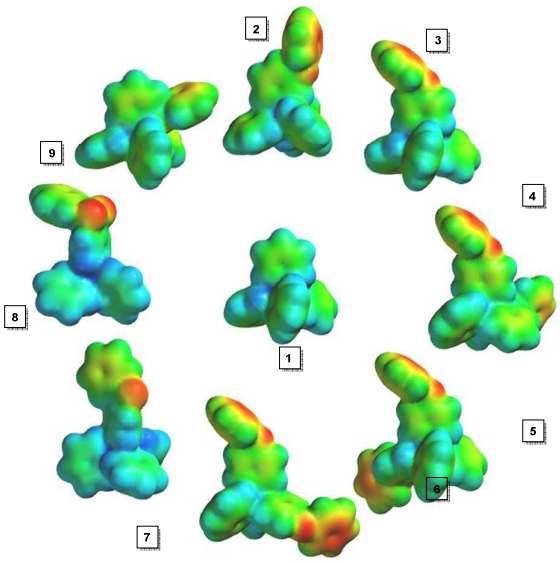

Figure 6. Electrostatic potential energy plots of cations corresponding to salts **1** – **9**. Common colour scale for **1**-**7**: 96 (red) to 387 (blue) kJ/mol; common scale for **8** and **9**: -4 (red) to 387 (blue) kJ/mol.

Cation geometries and electrostatic potentials

Optimized structures and electrostatic potential energy maps (elstats) of cations **1**-**9** as determined by the B3LYP/6-31G* model are shown in Figure 6; elstat ranges are summarized in Table 4. Dipole moments are presented in Table 5.

PPh_4^+, the cation of the parent salt **1**, is the simplest and most symmetric (S_4 point group), and its properties are presented as a reference for the series. The elstat energies on the surface of **1** range from 216 to 372 kJ/mol, with maxima near the central phosphorous; the least-positive values are on the faces of phenyl groups, with typical values ranging from 220 to 250 kJ/mol. The maximum elstat values are found near the phosphorus atom in all cations of the series.

The *ortho*-substituted cation of **2** adopts a "tucked" conformation (Figure 6), which hides the lone pairs of the phenoxy oxygen, limiting their external exposure and potential for interaction with other cations. For **2**, the elstat values span from 145 to 350 kJ/mol – a lower range than that of **1**, but

View Article Online
DOI: 10.1039/C7CP06278H

with a substantially higher floor as compared to **3** or **4**. The least-positive values are located on the π faces of the distal phenoxy moiety, where values range typically from 155 to 170 kJ/mol for either the *syn* or *anti* face (*syn*/*anti* - relative position of the π face to the lone pair region of the oxygen). Values on the π faces of the three unsubstituted phenyl groups range roughly from 210 to 230 kJ/mol, while the π faces of the substituted phenyl group on the central phosphorous fall in a similar range.

Cation from Salt:	Surface Elstat Range (kJ/mol)		Difference from **2** (kJ/mol)	
	Lowest	Highest	Lowest	Highest
1	+216	+372	+71	+22
2	+145	+350	-	-
3	+111	+361	-34	+11
4	+103	+359	-42	+9
5	+96	+337		
6	+97	+347		
7	+96	+345		
8	+16	+373		
9	-4	+387		

Table 4. Comparison of the most and least positive elstat values on the surfaces of the four cations, along with how the surface charges in **1**, **3** and **4** compared to that of **2**.

Table 5. Dipole moments of cations.[1]

Cation from Salt:	Dipole Moment (Debye)
1	0.00
2	2.25
3	4.79
4	5.09
5	4.47
6	3.91
7	4.79
8	7.94
9	11.76

[1]B3LYP/6-31G* model. Origin located at centre of nuclear charge.

The *meta*-substituted cation of **3** adopts an elongated geometry with both π faces and phenoxy oxygen lone pairs accessible for interaction. The elstat energies range from 111 to 361 kJ/mol. The least-positive sites are located on the lone pair region of the oxygen (~118 kJ/mol) and on the *syn* π face of the phenoxy moiety, where typical values range from 115 to 130 kJ/mol. Another less-positive region is located on the *anti* π face of phenoxy group, with representative values ranging from 135 to 150 kJ/mol. Values on π faces of the three central phenyl groups and on the faces of the substituted central phenyl group are analogous to that of **2**.

The elstat values of the *para*-substituted cation of **4** span a range of 103 to 359 kJ/mol, with least-positive sites at the lone pair region of the oxygen (~105 kJ/mol) and on the *syn* π face of the phenoxy moiety (115-135 kJ/mol). Another less-positive region of the cation is located on the *anti* π face of the distal phenoxy (145-155 kJ/mol). Values on the other π faces are analogous to that of **2** and **3**.

The dual-substituted cations **5**-**7** have similar surface elstat energies (ca. 96 to 343 kJ/mol) that fall below the ranges of **2** and **3**. The least-positive sites are at the *para* phenoxy oxygens (~100 kJ/mol), followed by the *meta* phenoxy oxygen of **6** at about 110 kJ/mol. As in **2**, the lone pair region of the *ortho* phenyoxy oxygen of **6** faces the interior of the cation and is largely hidden. Typical elstat values on the unsubstituted phenyl groups of **5**-**7** are ~10-15 kJ/mol lower than that found on cations **2**-**4**.

The ketone and sulfone moieties in respective cations **8** and **9** greatly impact the low end of the elstat range versus that of **1**. In the case of **8**, the elstat value is minimal at the carbonyl oxygen (16 kJ/mol); negative elstat values are found at the sulfone oxygens of **9** (-4 kJ/mol), suggesting that a favourable electrostatic interaction with another cation is possible through the sulfone. The *syn* π faces are also less-positive regions, with typical values of 130-140 kJ/mol on that of **9** and, 120-130 kJ/mol on that of **8**. Interestingly, the elstat values on the π faces of the unsubstituted phenyl groups of **8** and **9** more closely resemble those of **1** than of the phenoxy series **2**-**4**.

Molecular Dynamics Results

The structure of the different ILs was assessed using radial distribution functions (rdf), which are displayed in Figure 7. These functions were averaged over the range of 400-500 K, in which range the ILs remained in the liquid state. Furthermore, no significant variations in the values could be detected over this range. Figure 7a shows the rdf between the phosphorous atom of the cation and the nitrogen atom of the anion for the different ILs. Most of the variation between the different ILs occurs in the far shoulder of the first peak at around 9 Å, which corresponds to the tip of the functionalized phenyl group. The height of this shoulder follows the following order: **2** > **1**,**3** > **4** > **8**,**9** > **7**. Figure 7b shows the rdf between the phosphorous atom of the cation and the connecting atom of the functionalized phenyl group on the cation. This rdf can be viewed as a form of orientational alignment of the IL cations. Salt **2**, which does not show a first peak at 6 Å, shows no noticeable alignment of cations with other cations. This ordering increases in going to **3**, **7**, **4**, **8** and **9**. Interestingly, this increase in cation-cation ordering is also strongly correlated with the reduction in the T_m and reinforces the idea that "electrostatic exposure" has a significant effect on the IL properties. Salt **9** is the only IL that does not show this strong correlation between cation ordering and a lowering of T_m. However, in the following section, we show that the addition

View Article Online
DOI: 10.1039/C7CP06278H

of the sulfonyl linker leads to a very strong cation-cation ordering that makes it fundamentally different from the other ILs.

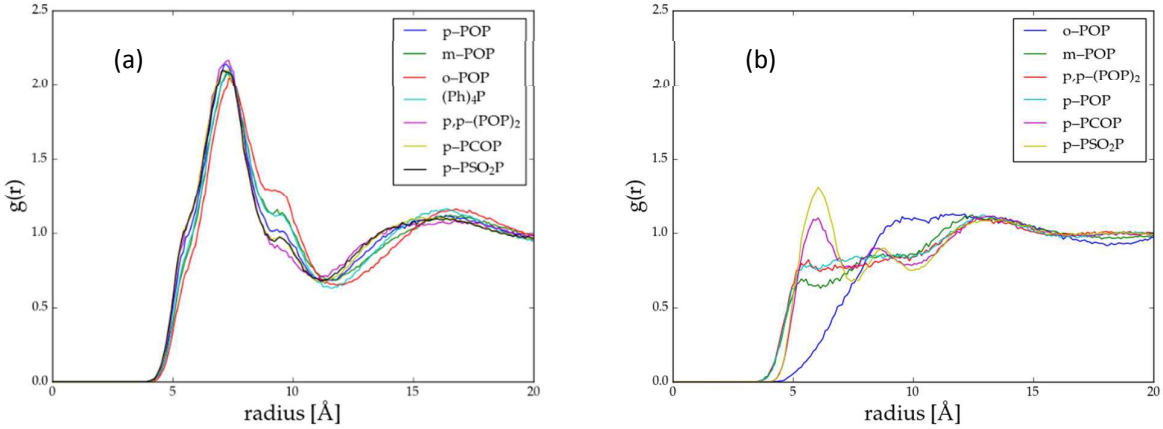

Figure 7. Radial distribution functions between (a) the phospohorous center of the cation and the anion's nitrogen and (b) the cation's phosphorous and the linking atom of the Ph-(R)-Ph group.

To assess the IL structures in further detail, spatial distribution functions (sdf) were constructed (see Figure 8) showing the preferred three-dimensional locations of the anion nitrogen (blue) and the cation phosphorous (orange) relative to the cation. The top row shows locations that are 3.5 times the bulk probability and the bottom row 2 times. Notice in Figure 8 that **2** has a near perfect tetragonal structure with anions strongly preferring to reside in the four crevices of the tetragonal cation (top), and secondarily at the tips of the phenyl groups (bottom). These two locations correspond to the first peak and the far shoulder of the rdf in Figure 7a. Both **3** and **4** show a significant loss of anion localization at the apex of the functionalized phenyl group. This coincides with the reduction in the rdf shoulder height in Figure 7a and further supports the idea that articulation of the phenoxy group might frustrate order in this direction, driving down T_m. Salts **8** and **9** additionally show significant ordering of secondary cations (orange in Figure 8) near the functionalized phenyl group. Note that **8** does this in a way that does not disrupt cation-anion structure at the top tip of the cation, while this location is completely blocked in **9**, again suggesting a fundamentally different liquid structure for the latter.

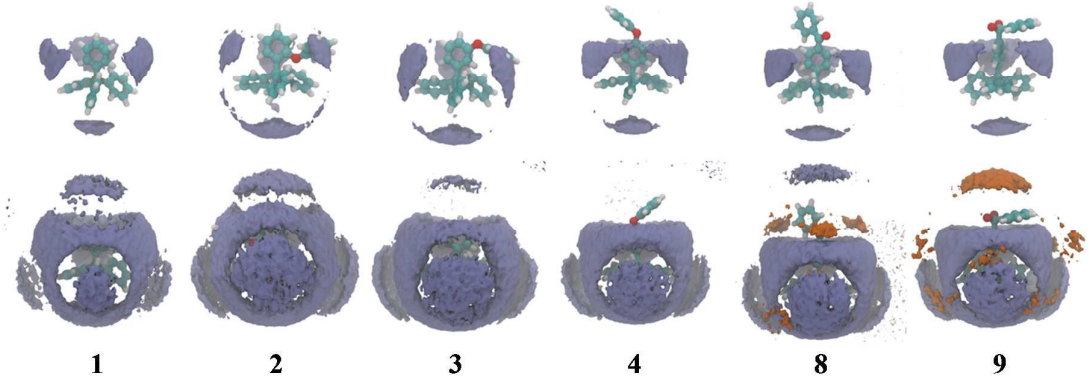

Figure 8. Spatial distribution functions showing the preferred locations of nitrogen atoms of the anion (blue) and the phosphorous atoms of other cations (orange) relative to the cation. The top row show surfaces that are 3.5 times the bulk density and the bottom row 2 times the density.

The enthalpy of the liquid state as a function of temperature for each of the ILs is given in Figure 9. Salt **3** has the lowest enthalpy of the cations, followed by **1**, **4**, **7** and then **2**. Additionally, salts **8** and **9** have the highest enthalpy of the ILs.

View Article Online
DOI: 10.1039/C7CP06278H

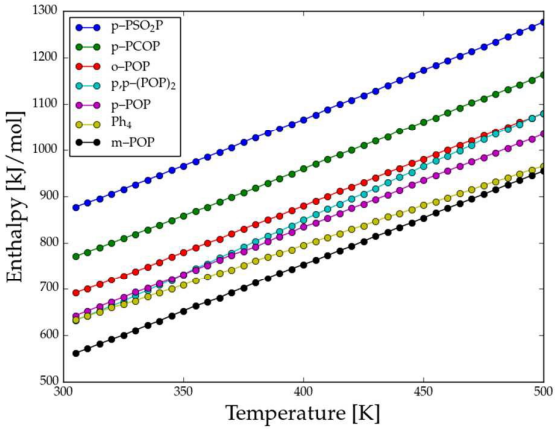

Figure 9. Liquid phase enthalpy as a function of temperature for the different salts.

Table 6 shows the liquid phase entropy of salts **1**, **2** and **4** at selected temperatures using the two-phase thermodynamic method (see Supporting Information for details).[36-38] As one might expect, these values are larger at the higher temperatures, but there is little difference between the three ILs. The bulk contribution to the entropy comes from vibrational components (>65%) and, in comparing **1** vs. **2** and **4**, appears proportional to the number of vibrational degrees of freedom.

Salt	Temp (K)	S_{trans} (J/mol K)	S_{rot} (J/mol K)	S_{vib} (J/mol K)	S_{total} (J/mol K)
1	400	168	163	629	960
2	300	144	138	551	832
	400	169	167	761	1097
	500	193	187	937	1318
4	300	141	137	557	835
	400	168	164	761	1093
	500	193	188	946	1327

Table 6. Liquid phase entropy as a function of temperature as computed by the two-phase thermodynamic method.

Type	**1→2** (vdw,elec)	**1→3** (vdw,elec)	**1→4** (vdw,elec)
cation-cation	+14.0 (-6.4,+20.4)	-48.0 (-7.4,-40.6)	+0.1 (-7.9,+8.0)
cation-anion	-0.4 (-3.1,+2.7)	-0.5 (-4.8,+4.3)	-2.4 (-6.3,+3.9)
anion-anion	-10.1 (+1.7,-11.8)	-8.7 (+1.7,-10.4)	-8.4 (+2.0,-10.3)
total	+3.5 (-7.8,+11.3)	-57.2 (-10.5,-46.7)	-10.7 (-12.3,+1.6)

Table 7. Breakdown of the change in pairwise interaction energies, given in kJ/mol-pair, between the different ILs. Values in parenthesis are the van der Waals (vdw) and electrostatic (elec) contribution to the overall pairwise energy.

Table 7 shows a breakdown of the changes in the average pairwise interaction energies between the different ion types relative to **1**. Going from **1** to **2** is shown to be slightly unfavourable (+3.5 kJ/mol), which agrees with the increase in ΔH^{fus} that is seen from experiment (+18.2 kJ/mol). The breakdown shows that this is largely caused by an increase in cation-cation energy (+14.0 kJ/mol) and particularly the electrostatic contribution to this interaction (+20.4 kJ/mol). No significant change is seen for the cation-anion interaction (-0.4 kJ/mol). The anion-anion contribution, while more favourable (-10.1 kJ/mol – likely due to the increased lattice spacing due to the larger cation of **2**), is unable to overcome the large increase in cation-cation energy.

Going from **1** to **3** is predicted to be largely favourable, though there is no source of experimental confirmation for this, since **3** was never observed to crystallize. Regardless, this is predicted to be the case, driven by a strong decrease in the electrostatic component of the cation-cation interactions. Since the electrostatic interactions between the cations are entirely repulsive, this can be interpreted as a strong easing of this repulsion. In changing the phenoxy group from the *ortho*- to the *para*- position, the electronegative oxygen atom is pushed farther from the positive phosphorous centre, resulting in a larger electrostatic moment. Hence, through proper alignment, cations in **4** can take advantage of this dipole moment to significantly reduce the electrostatic repulsions, while cations in **2** are unable to do so effectively. This view agrees with the increase in the rdf peak in Figure 7b and could explain why there is a significantly weaker cation-cation electrostatic repulsion in **4** relative to **2**. Representative snapshots of these cation alignments are shown in Figure 10.
The MD results show that going from **1** to **4** is slightly favourable (-10.7 kJ/mol), and is driven by increased favourability of anion-anion interactions (-8.4 kJ/mol). The experiments show only a very slight increase in ΔH^{fus} between the two ILs (+1.5 kJ/mol). Again, it is reasoned that this lessening of electrostatic repulsions experienced by the anions is caused by increased lattice spacing resulting from the larger cation size.

Discussion of Computational Results

For the *ortho*-substituted cation (**2**), both quantum calculations and molecular dynamics simulations indicate that the phenoxy ring exists primarily in a bent or tucked configuration. The tucked configuration shields the lone pair of electrons on the phenoxy oxygen; consequently, the presented surface area of the *ortho*-substituted cation is more positive than that of either the *p*- or the *m*-substituted cations as shown in Table 4. Hence, the cation-cation interaction is more

View Article Online
DOI: 10.1039/C7CP06278H

repulsive in **2** and the more compact **2** is also presumably more efficiently packed in the crystalline lattice than is **4**, resulting in the greater enthalpy of fusion. For both the *ortho* (**2**) and *para*-substituted (**4**) cations, molecular dynamics simulations indicate liquid-phase entropies higher than that of **1**, in agreement with the higher entropy of fusion for **2** and **4** observed experimentally, as to be expected for a species with additional atoms, vibrations and rotations. Furthermore, the extended orientation of the phenoxy groups in salts **3** and **4** (again observed in both quantum and molecular dynamics calculations) support the concept that asymmetry imparted by an extended phenoxy group plays a role in the increase in the entropy of fusion, likely due to frustrated packing in the solid phase in addition to increased freedom in the liquid phase.

Taken as a whole, the results of the thermodynamic analysis, quantum calculations and molecular dynamics simulations present a complex yet complimentary picture of this family of thermally stable molten salts. Typically, with organic ions in common ionic liquids (*i.e.*, imidazolium or pyridinium cations), the addition of pendant moieties on a parent ion would be expected to marginally increase enthalpies of fusion (due to additional van der Waals interactions) and significantly increase the entropy of fusion by frustrating packing, resulting in melting point decreases. However, in this series of salts, the addition of pendant groups to the parent cation results in properties that appear to be largely governed by differences in cation-cation interactions.

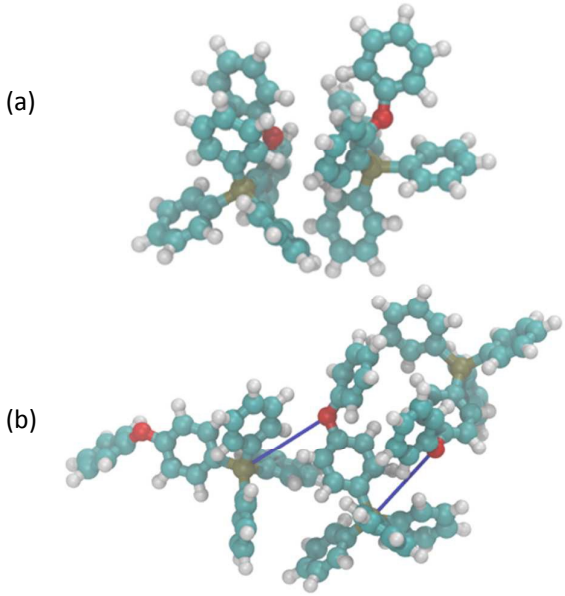

Figure 10. Representative snapshots showing (a) the failure of two close cations of salt **2** to form an energetic pair and (b) three cations of salt **4** forming an oriented trimer. Blue lines show favourable alignments between oxygen atoms and phosphorous atoms of separate cations.

Relative to the parent PPh_4^+ cation in **1** the introduction of a single phenoxy group on the cation can bring about electrostatic and structural effects that alter the enthalpy and entropy of fusion, and thus the melting point, in dramatically different ways, depending on the position of the substitution.[§§] While the *ortho*-substituted species **2** has it's phenoxy group in a tucked conformation that inhibits the electrostatic exposure of the lone electron pairs on the oxygen, the *meta*- (**3**) and *para*-substituted (**4**) species have extended phenoxy groups. This allows for significantly decreased cation-cation repulsion in **3** and slightly more cation-anion interaction in **4**. Quantum chemical calculations of the isolated cations show that **2** has a more positive exposed surface than does **3** or **4**. Similarly, the results from molecular dynamics simulations of the liquid phase show that the additional phenyl ring in **2** does, in fact, lower the Van der Waals interaction energy, as it allows for more π face interactions, however this effect is overwhelmed by the increase in the electrostatic cation-cation interaction, making the overall liquid phase cation-cation interaction less favourable (more repulsive) than in **1**. This, along with its larger cation size, serves to increase cation-cation interaction energy, which increases the liquid phase enthalpy and subsequently the observed enthalpy of fusion. As these effects overwhelm the entropy increases arising from asymmetry and additional atoms and bonds, the enthalpy increase becomes the driving force for the increase in melting point from **1** to **2**.

Conversely, when the phenoxy group is placed in the *para* position (**4**), molecular dynamics simulations show that the increase in electrostatic energy is much smaller, likely due to the electrostatic exposure of the lone electron pairs on the phenoxy oxygen. This increase in energy agrees with the quantum calculations of the isolated cation, and is virtually offset by the favourable Van der Waals interactions as seen in both the molecular dynamics simulations and in the experimental enthalpy of fusion. Here, entropy dominates a melting point decrease. The lack of an observable first-order solid/liquid transition for the *meta*-substituted cation (**3**) is consistent with the overall liquid phase energy (from MD) and isolated cation charge (from quantum calculations) of **3** being significantly lower than **1**, **2** or **4**. This decrease in energy relative to the other species is primarily driven by smaller cation-cation repulsion, also indicated by both quantum and MD calculations. This would lead to a lower enthalpy of fusion and, coupled with the asymmetry of the cation of **3**, could result in the formation of a gel or glass rather than an ordered solid.

To summarize, the relationship between T_m and substituents on a core phenyl ring of the parent PPh_4^+ cation is less obvious than one of simple substitution position; rather, it is tied more closely to how the substitution affects the electronics and structure of the cation, and in turn how these affect the liquid phase properties. In general, with cation-anion interactions

View Article Online
DOI: 10.1039/C7CP06278H

being similar among the phenoxy-substituted species (**2**, **3** and **4**) the melting point decreases as the cation-cation repulsive interactions are decreased. Species **7**, which contains the bis-*para*-phenoxy substituted cation has a melting point and thermodynamic properties very similar to **4**, with slightly higher enthalpy and enthalpy, as would be expected from adding another bulky phenoxy group. The nexus between the strength of the cation-cation interaction and melting point is continued with **8**, where substitution is at the *para* position, but the linking group is a carbonyl group rather than an oxygen atom. Radial distribution functions between cation centres and the linker atoms of different cations suggest that this reduction in cation-cation repulsions is a result of the alignment of electrostatic moments between the neighbouring cations. But, we note that compound **9**, which has the highest alignment, is fundamentally different from the other salts in its liquid phase structure, because of an unusually strong cation-cation orientation that prevents formation of the tetragonal structure that is common to the other cations.

Conclusions

The present results make it clear that the Tf_2N^- salts of the herein-described PPh_4^+- based cations are materials of truly remarkable thermal stability, being unaltered by heating, in the presence of air, at 300°C for three months; indeed, based upon the post-heating analysis of these salts, we have little doubt that they would be stable indefinitely at that temperature or perhaps ones even higher. This is especially significant in light of the fact that, under identical conditions, commercial samples of the 'high-performance' polymers PEEK and PES were – at least by inspection – visibly more degraded than were the present ionic liquids. In all, the new salts described here may be the most thermally stable organic materials heretofore described, or certainly amongst them. This augurs well for their suitability for use in a host of high-temperature applications.

From a more fundamental standpoint, the present findings lead us to conclude that for relatively rigid, structurally similar cations (roughly the same number of substituents, effective size, sterics, *etc.*), increasing the electric dipole moment of the cation allows them to align when in the liquid state, leading to a more stable liquid state and, consequently, a lower melting point; However, *if* the dipole moment introduced by the structural modification is *too* strong (as is the case with sulfonyl per the present report) significant changes take place in the liquid state (and perhaps the solid state as well) that worsen the thermodynamics of melting. Clearly, then, achieving a balance between these considerations is to be sought in their ongoing development. To that end, we have begun the synthesis of new salts intended to further test and refine this hypothesis, and we expect to report those results in due course.

Acknowledgements

This material is based upon work supported by the National Science Foundation under grant number CHE-1464740. JHD also thanks the donors of the Petroleum Research Fund, administered by the American Chemical Society, for support of this research. Finally, this work was also made possible in part by a grant of high performance computing resources and technical support from the Alabama Supercomputer Authority.

Notes and references

§ Frontier Scientific, Inc., Logan, UT, USA.

§§ We note that in a related work by our group (accepted for publication pending revision), the position of substitution on the quinoline ring in a family of (quinoline)$PPh_3^+Tf_2N^-$ ILs plays a critical role in the thermal stability of the individual isomers.

References

1. G. Baum and F. R. Short, *Thermal stability of organic compounds determined by the isoteniscope method*, Technical Report No. AFML-TR-65-347, Air Force Materials Laboratory,Wright-Patterson Air Force Base, 1966.
2. E. S. Blake, W. C. Hammann, J. W. Edwards, T. E. Reichard and M. R. Ort, *J. Chem. Eng. Data*, 1961, **6**, 87.
3. I. B. Johns, E. A. McElhill and J. O. Smith, *Ind. Eng. Chem. Prod. Res. Dev.*, 1962, **1**, 2.
4. I. B. Johns, E. A. McElhill and J. O. Smith, *Journal of Chemical & Engineering Data*, 1962, **7**, 277.
5. J. J. Madison and R. M. Roberts, *Ind. Eng. Chem.*, 1958, **50**, 237.
6. P. E. Cassidy, *Thermally Stable Polymers: Synthesis and Properties*, Marcel Dekker, Inc., 1980.
7. C. S. Marvel. In *Proc. Stabil. Plast., Soc. Plast. Eng. Reg. Tech. Conf.*; H. Lenheis, Ed: Washington, D.C., 1967.
8. C. S. Marvel, *J. Macromol. Sci., Part A*, 1967, **1**, 7.
9. C. S. Marvel, *Pure Appl. Chem.*, 1968, **16**, 351.
10. C. S. Marvel, *Appl. Polym. Symp.*, 1973, **No. 22**, 47.
11. A. H. Tullo, *Chem. Eng. News*, 2016, **94** (9), 23.
12. C. G. Cassity, A. Mirjafari, N. Mobarrez, K. J. Strickland, R. A. O'Brien and J. H. Davis, *Chem. Commun.*, 2013, **49**, 7590.
13. C. Maton, N. De Vos and C. V. Stevens, *Chem. Soc. Rev.*, 2013, **42**, 5963.
14. K. J. Fraser , D. R. MacFarlane, *Aust. J. Chem.*, 2009, **62**, 309 .
15. C. J. Bradaric, A. Downard, C. Kennedy, A. J. Robertson, Y. Zhou, *Green Chem.*, 2003, **5**, 143.
16. M. Scheuermeyer, M. Kusche, F. Agel, P. Schreiber, F. Maier, H.-P. Steinrueck, J. H. Davis, F. Heym, A. Jess and P. Wasserscheid, *New J. Chem.*, 2016, **40**, 7157.
17. C. A. Corley, R. E. Del Sesto, J. S. Wilkes, *Proc. - Electrochem. Soc.*, 2004, **24**, 326.
18. R. E. Del Sesto, C. Corley, A. Robertson, J. S. Wilkes, *J. Organomet. Chem.*, 2005, **690**, 2536.
19. B. Siu, C. G. Cassity, A. Benchea, T. Hamby, J. Hendrich, K. J. Strickland, A. Wierzbicki, R. E. Sykora, E. A. Salter, R. A. O'Brien, K. N. West and J. H. Davis, Jr., *RSC Adv.*, 2017, **7**, 7623.
20. A. Benchea, B. Siu, M. Soltani, J. H. McCants, E. A. Salter, A. Wierzbicki, K. N. West and J. H. Davis, Jr., *New J. Chem.*, 2017, **41**, 7844.

View Article Online
DOI: 10.1039/C7CP06278H

21. D. Marcoux and A. B. Charette, *Adv. Synth. Catal.*, 2008, **350**, 2967.
22. E. B. Fox, L. T. Smith, T. K. Williamson, S. E. Kendrick, *Energy & Fuels*, 2013, **27**, 6355.
23. A. D. Becke, *J. Chem. Phys.*, 1993, **98**, 5648.
24. C. Lee, W. Yang and R. G. Parr, *Phys. Rev. B: Condens. Matter*, 1988, **37**, 785.
25. P. J. Stephens, F. J. Devlin, C. F. Chabalowski and M. J. Frisch, *J. Phys. Chem.*, 1994, **98**, 11623.
26. S. H. Vosko, L. Wilk and M. Nusair, *Can. J. Phys.*, 1980, **58**, 1200.
27. J. Wang, R. M. Wolf, J. W. Caldwell, P. A. Kollman and D. A. Case, *J. Comput. Chem.*, 2004, **25**, 1157.
28. M. J. Frisch, G. W. Trucks, H. B. Schlegel, G. E. Scuseria, M. A. Robb, J. R. Cheeseman, G. Scalmani, V. Barone, B. Mennucci, G. A. Petersson, H. Nakatsuji, M. Caricato, X. Li, H. P. Hratchian, A. F. Izmaylov, J. Bloino, G. Zheng, J. L. Sonnenberg, M. Hada, M. Ehara, K. Toyota, R. Fukuda, J. Hasegawa, M. Ishida, T. Nakajima, Y. Honda, O. Kitao, H. Nakai, T. Vreven, J. A. Montgomery, J. E. Peralta, F. Ogliaro, M. Bearpark, J. J. Heyd, E. Brothers, K. N. Kudin, V. N. Staroverov, R. Kobayashi, J. Normand, K. Raghavachari, A. Rendell, J. C. Burant, S. S. Iyengar, J. Tomasi, M. Cossi, N. Rega, J. M. Millam, M. Klene, J. E. Knox, J. B. Cross, V. Bakken, C. Adamo, J. Jaramillo, R. Gomperts, R. E. Stratmann, O. Yazyev, A. J. Austin, R. Cammi, C. Pomelli, J. W. Ochterski, R. L. Martin, K. Morokuma, V. G. Zakrzewski, G. A. Voth, P. Salvador, J. J. Dannenberg, S. Dapprich, A. D. Daniels, Farkas, J. B. Foresman, J. V. Ortiz, J. Cioslowski and D. J. Fox, *Gaussian 09, Revision E.01,* Gaussian, Inc., Wallingford CT, 2009
29. K. G. Sprenger, V. W. Jaeger and J. Pfaendtner, *J. Phys. Chem. B*, 2015, **119**, 5882.
30. L. Martinez, R. Andrade, E. G. Birgin and J. M. Martinez, *J. Comput. Chem.*, 2009, **30**, 2157.
31. S. Plimpton, *J. Comput. Phys.*, 1995, **117**, 1.
32. R. W. Hockney and J. W. Eastwood, *Computer Simulation Using Particles*, CRC Press - Taylor & Francis Group, New York, NY, 1998.
33. M. J. Earle, J. M. S. S. Esperanca, M. A. Gilea, J. N. Canongia Lopes, L. P. N. Rebelo, J. W. Magee, K. R. Seddon and J. A. Widegren, *Nature*, 2006, **439**, 831.
34. R. A. O'Brien, A. Mirjafari, K. M. Mattson, S. M. Murray, N. Mobarrez, E. A. Salter, A. Wierzbicki, J. H. Davis and K. N. West, *J. Phys. Chem. B*, 2014, **118**, 10232.
35. S. M. Murray, R. A. O'Brien, K. M. Mattson, C. Ceccarelli, R. E. Sykora, K. N. West and J. H. Davis, Jr., *Angew. Chem., Int. Ed.*, 2010, **49**, 2755.
36. S.-T. Lin, M. Blanco and W. A. Goddard, III, *J. Chem. Phys.*, 2003, **119**, 11792.
37. S.-T. Lin, P. K. Maiti and W. A. Goddard, III, *J. Phys. Chem. B*, 2010, **114**, 8191.
38. T. A. Pascal, S.-T. Lin and W. A. Goddard, III, *Phys. Chem. Chem. Phys.*, 2011, **13**, 169